World Academy of Science, Engineering and Technology
International Journal of Physical and Mathematical Sciences
Vol:2, No:12, 2008

Towards finite element modeling of the accoustics of human head

Maciej Paszyński, Leszek Demkowicz, Jason Kurtz

Abstract—In this paper, a new formulation for acoustics coupled with linear elasticity is presented. The primary objective of the work is to develop a three dimensional *hp* adaptive finite element method code destinated for modeling of acoustics of human head. The code will have numerous applications e.g. in designing hearing protection devices for individuals working in high noise environments. The presented work is in the preliminary stage. The variational formulation has been implemented and tested on a sequence of meshes with concentric multi-layer spheres, with material data representing the tissue (the brain), skull and the air. Thus, an efficient solver for coupled elasticity/acoustics problems has been developed, and tested on high contrast material data representing the human head.

Keywords—finite element method, acoustics, coupled problems, biomechanics

I. Introduction

THIS paper presents preliminary results of the long-term project towards development of the acoustics of the human head. The adaptive finite element method utilize in the project seem to provide more reliable and accurate results than previous attempts based on the boundary element method [15].

The focus of this project is to to develop a reliable numerical model for investigating the bone-conducted sound in the human head. The problem is difficult because of a lack of fundamental knowledge regarding the transmission of acoustic energy through non-airborne pathways to the cochlea. A fully coupled model based on the acoustic/elastic interaction problem with a detailed resolution of the cochlea region and its interface with the skull and the air pathways, should provide an insight into this fundamental, long standing research problem.

II. Formulation of the Coupled Elasticity/Acoustics Problem

In this opening section, the derivation of the variational formulations for acoustics, elasticity and then for the ultimate coupled elasticity/acoustics problem is presented.

A. Linear Acoustics Equations

The classical linear acoustics equations are obtained by linearizing the isentropic form of the compressible Euler equations expressed in terms of density ρ and velocity vector v_i, around the hydrostatic equilibrium position $\rho = \rho_0, v_i = 0$. Perturbing the solution around the equilibrium position,

$$\rho = \rho_0 + \delta\rho, \quad v_i = 0 + \delta v_i,$$

and linearizing the Euler equations, see e.g. [6], results in a system of four first order equations in terms of unknown perturbations of density $\delta\rho$ and velocity δv_i,

$$\begin{cases} (\delta\rho)_{,t} + \rho_0(\delta v_j)_{,j} = 0 \\ \rho_0(\delta v_i)_{,t} + (\delta p)_{,i} = 0\,, \end{cases}$$

with δp denoting the perturbation in pressure. For the isentropic[1] flow, the pressure is simply an algebraic function of density,

$$p = p(\rho)$$

Linearization around the equilibrium position leads to the relation between the perturbation in density and the corresponding perturbation in pressure

$$p = \underbrace{p(\rho_0)}_{p_0} + \frac{dp}{d\rho}(\rho_0)\delta\rho$$

Here p_0 is the hydrostatic pressure, and the derivative $\frac{dp}{d\rho}(\rho_0)$ is interpreted *a posteriori* as the sound speed squared, and denoted by c^2. Consequently, the perturbation in pressure and density are related by the simple linear equation,

$$\delta p = c^2\delta\rho$$

It is customary to express the equations of linear acoustics in pressure rather than density. Dropping deltas in the notation results in,

$$\begin{cases} c^{-2}p_{,t} & +\rho_0 v_{j,j} & = 0 \\ \rho_0 v_{i,t} & +p_{,i} & = 0 \end{cases}$$

In this report, only time-harmonic problems are considered. The ansatz,

$$p(t,\boldsymbol{x}) = e^{i\omega t}p(\boldsymbol{x}), \quad u_i(t,\boldsymbol{x}) = e^{i\omega t}u_i(\boldsymbol{x})\,,$$

is assumed to reduce the acoustics equations to,

$$\begin{cases} c^{-2}i\omega p & +\rho_0 v_{j,j} & = 0 \\ \rho_0 i\omega v_i & +p_{,i} & = 0 \end{cases}$$

Maciej Paszyński is with the Department of Computer Science, AGH University of Science and Technology, Krakow, Poland, email: paszynsk@agh.edu.pl
Leszek Demkowicz is with the Institute for Computational Engineering and Sciences, The University of Texas at Austin, USA, email: leszek@ices.utexas.edu
Jason Kurtz is with the Institute for Computational Engineering and Sciences, The University of Texas at Austin, USA, email: kurtzj@ices.utexas.edu

[1]The entropy is assumed to be constant throughout the whole domain

or in the operator form,

$$\begin{cases} c^{-2}i\omega p & +\rho_0 \boldsymbol{\nabla}\cdot\boldsymbol{v} & = 0 \\ \rho_0 i\omega v_i & +\boldsymbol{\nabla} p & = 0 \end{cases}$$

The velocity is then eliminated to obtain the Helmholtz equation for the pressure,

$$-\Delta p - k^2 p = 0 \,,$$

with the wave number $k = \omega/c$.

Having obtained the second order problem, the derivation of the weak formulation can be proceed. It is a little more iluminating to obtain the same variational formulation starting with the first order system. First of all, a clear choice in a way the two equations are treated, must be made. The equation of continuity (conservation of mass) is going to be satisfied only in the *weak sense*, i.e. by multiplying it with a test function q, integrate over domain Ω and integrating the second term by parts to obtain,

$$\int_\Omega \left(\frac{i\omega}{c^2} pq - \rho_0 \boldsymbol{v}\boldsymbol{\nabla} q\right) \, d\boldsymbol{x} + \rho_0 \int_\Gamma v_n q \, dS = 0, \quad \forall q$$

Here $v_n = v_j n_j$ denotes the normal component of the velocity on the boundary.

The second equation (conservation of momentum) is satisfied in the *strong sense*, i.e. pointwise. Solving for the velocity, results in

$$\boldsymbol{v} = -\frac{1}{\rho_0 i\omega}\boldsymbol{\nabla} p$$

In particular, the normal component of the velocity is related to the normal derivative of the pressure,

$$v_n = -\frac{1}{\rho_0 i\omega}\frac{\partial p}{\partial n}$$

At this point different boundary conditions are introduced:

- a soft boundary Γ_D,
$$p = p_0$$
- a hard boundary Γ_N,
$$v_n = v_0$$
- and an impedance condition with a constant $d > 0$,
$$v_n = dp + v_0$$

Multiplying Equation II-A with $i\omega$, substituting the boundary data into the boundary term, and eliminating the velocity in the domain integral term, using formula II-A, results in the final variational formulation.

$$\begin{cases} p = p_0 \text{ on } \Gamma_D \\ \displaystyle\int_\Omega \left(\boldsymbol{\nabla} p \boldsymbol{\nabla} q - \left(\frac{\omega}{c}\right)^2 pq\right) \, d\boldsymbol{x} + \\ \displaystyle i\omega\rho_0 d \int_{\Gamma_C} pq \, dS = \\ \displaystyle -\int_{\Gamma_N\cup\Gamma_C} v_0 q \, dS \\ \forall q \;:\; q = 0 \text{ on } \Gamma_D \end{cases}$$

The weak formulation has been obtained without introducing the second order problem at all! It is clear which of the starting equations is understood in the weak, and which in a strong sense. The momentum equations, consistently with their pointwise interpretation, have been extended to the boundary to yield the appropriate boundary conditions. It should be emphasized All these considerations can be made more precise by introducing the language of distributions and Sobolev spaces.

B. Linear Elasticity

The time-harmonic linear elasticity equations include:

- balance of momentum,
$$-\rho\omega^2 u_i - \sigma_{ij,j} = f_i$$
- Cauchy displacement-strain relation,
$$\epsilon_{ij} = \frac{1}{2}(u_{i,j} + u_{j,i})$$
- consititutive law,
$$\sigma_{ij} = E_{ijkl}\epsilon_{kl}$$

The tensor of elasticities satisfies the usual symmetry assumptions,

$$E_{ijkl} = E_{jikl}\,, \quad E_{ijkl} = E_{ijlk}\,, \quad E_{ijkl} = E_{klij}\;.$$

In the case of an isotropic material,

$$E_{ijkl} = \mu(\delta_{ik}\delta_{jl} + \delta_{il}\delta_{jk}) + \lambda\delta_{ij}\delta_{kl}$$

and the constitutive law reduces to the Hooke's law,

$$\sigma_{ij} = 2\mu\epsilon_{ij} + \lambda\epsilon_{kk}\delta_{ij}$$

Utilizing the Cauchy geometric relations, we eliminate the strain tensor and represent the stresses directly in terms of the displacement gradient,

$$\sigma_{ij} = E_{ijkl} u_{k,l} \tag{1}$$

or, for the Hooke's law,

$$\sigma_{ij} = \mu u_{i,j} + \lambda u_{k,k}\delta_{ij} \tag{2}$$

The momentum equations will be satisfied in the weak sense. We multiply them with a test function v_i, integrate over Ω and integrate by parts to obtain,

$$\int_\Omega \left(\sigma_{ij} v_{i,j} - \rho\omega^2 u_i v_i\right) \, d\boldsymbol{x} - \int_\Gamma \sigma_{ij} n_j v_i \, dS = \int_\Omega f_i v_i \, d\boldsymbol{x}, \quad \forall v_i \tag{3}$$

The boundary conditions can be introduced now:

- prescribed displacements on Γ_D,
$$u_i = u_{i,D}$$
- prescribed tractions on Γ_N,
$$t_i := \sigma_{ij} n_j = g_i$$
- prescribed impedance on Γ_C,
$$t_i + \beta_{ij} u_j = g_i$$

The consideration are restricted now to $v_i = 0$ on Γ_D. The boundary data into the boundary term in Equation 3 are substituted to obtain,

$$\begin{cases} \int_\Omega \left(\sigma_{ij} v_{i,j} - \rho\omega^2 u_i v_i\right)\, d\boldsymbol{x} + \\ \int_{\Gamma_C} \beta_{ij} u_j v_i \, dS = \\ \int_\Omega f_i v_i \, d\boldsymbol{x} + \int_{\Gamma_N \cup \Gamma_C} g_i v_i \, dS \\ \qquad \forall v_i \;:\; v_i = 0 \text{ on } \Gamma_D \end{cases} \tag{4}$$

The final variational formulation is obtained by substituting formula 1 for stresses,

$$\begin{cases} u_i = u_{i,D} \text{ on } \Gamma_D \\ \int_\Omega \left(E_{ijkl} u_{k,l} v_{i,j} - \rho\omega^2 u_i v_i\right)\, d\boldsymbol{x} + \\ \int_{\Gamma_C} \beta_{ij} u_j v_i \, dS = \\ \int_\Omega f_i v_i \, d\boldsymbol{x} + \int_{\Gamma_N \cup \Gamma_C} g_i v_i \, dS \\ \qquad \forall v_i \;:\; v_i = 0 \text{ on } \Gamma_D \end{cases} \tag{5}$$

The final fomulas for the bilinear and linear forms are recorded.

$$\begin{aligned} X &= \boldsymbol{H}^1(\Omega) := (H^1(\Omega))^3 \\ b(\boldsymbol{u}, \boldsymbol{v}) &= \int_\Omega \left(E_{ijkl} u_{k,l} v_{i,j} - \rho\omega^2 u_i v_i\right)\, d\boldsymbol{x} + \\ &\quad \int_{\Gamma_C} \beta_{ij} u_j v_i \, dS \\ l(\boldsymbol{v}) &= \int_\Omega f_i v_i \, d\boldsymbol{x} + \int_{\Gamma_N \cup \Gamma_C} g_i v_i \, dS \end{aligned} \tag{6}$$

C. Elasticity Coupled with Acoustics

Let Ω be a domain in $\mathbb{R}^3$. In the following discussion it is assumed that the domain Ω is bounded. The Ω is split into two disjoint parts: a subdomain Ω_e occupied by a linear elastic medium, and a subdomain Ω_a occupied by an acoustical fluid. The two subdomains are separated by an interface Γ_I. Neither the subdomains nor the interface need to be connected (they may consist of several separate pieces). The external boundary $\partial\Omega$ will be partitioned into Dirichlet, Neumann and Cauchy parts: $\Gamma_D, \Gamma_N, \Gamma_C$, respectively. Each of these boundary parts may consist of a part belonging to the boundary $\partial\Omega_e$ of the elastic subdomain, or the boundary $\partial\Omega_a$ of the acoustical subdomain. Using a more precise mathematical language, Ω_e, Ω_a are assumed to be opened and disjoint and,

$$\overline{\Omega} = \overline{\Omega}_e \cup \overline{\Omega}_a \,.$$

Similarly, elastic and acoustics parts of the Dirichlet boundary: $\Gamma_{De}, \Gamma Da$, of the Neumann boundary: $\Gamma_{Ne}, \Gamma Na$, and the Cauchy boundary: $\Gamma_{Ce}, \Gamma Ca$, are open submanifolds of $\partial\Omega$ and,

$$\partial\Omega = \overline{\Gamma}_{De} \cup \overline{\Gamma}_{Da} \cup \overline{\Gamma}_{Ne} \cup \overline{\Gamma}_{Na} \cup \overline{\Gamma}_{Ce} \cup \overline{\Gamma}_{Ca} \,,$$

as well as,

$$\partial\Omega_e = \overline{\Gamma}_I \cup \overline{\Gamma}_{De} \cup \overline{\Gamma}_{Ne} \cup \overline{\Gamma}_{Ce} \quad \partial\Omega_a = \overline{\Gamma}_I \cup \overline{\Gamma}_{Da} \cup \overline{\Gamma}_{Na} \cup \overline{\Gamma}_{Ca} \,.$$

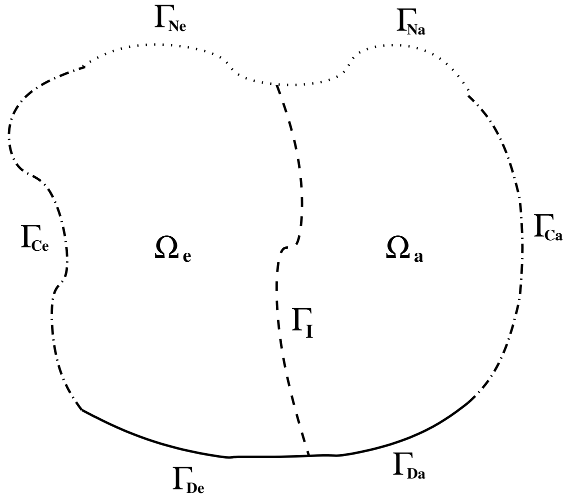

Fig. 1. Topology of a coupled problem

A two-dimensional illustration of the scenario is shown in Figure 1. The coupled problem involves solving linear elasticity equations discussed in Section II-B satisfied in subdomain Ω_e coupled with the equations of linear acoustics discussed in Section II-A and satisfied in subdomain Ω_a. The unknowns include the components of the displacement vector $u_i(\boldsymbol{x}), \boldsymbol{x} \in \overline{\Omega}_e$ and the acoustical pressure $p(\boldsymbol{x}), \boldsymbol{x} \in \overline{\Omega}_a$. The two sets of equations are accompanied by appropriate boundary conditions and coupled by the following interface conditions:

$$\begin{aligned} i\omega u_i n_i = v_i n_i &= -\frac{1}{\rho_f i\omega}\frac{\partial p}{\partial x_i} n_i, \\ t_i = \sigma_{ij} n_j &= -p n_i \end{aligned} \tag{7}$$

The first equation above expresses the continuity of normal component of the velocity: the normal elastic velocity has to match the normal component of the acoustical velocity. The second equation expresses the continuity of stresses: the normal elastic stress must be equal to the (negative) pressure, whereas the tangential component of the elastic stress vector is set to zero, since the fluid does not support a shear stress. As usual, ω is the angular frequency, i is the imaginary unit, ρ_f stands for the density of the fluid, and n_i denote components of a unit vector normal to interface Γ_I assumed to be directed from the elastic into the acoustical subdomain. Multiplying the first interface condition by $\rho_f i\omega$, we get,

$$\rho_f \omega^2 u_n = \frac{\partial p}{\partial n}, \quad t_i = \sigma_{ij} n_j = -p n_i$$

where $u_n = u_i n_i$ denotes the normal displacement. From the mathematical point of view, the conditions of this type are classified as *weak coupling conditions*. The word “weak” refers here to the fact that the primary variable for elasticity - the displacement vector, matches the secondary variable (the flux) for the acoustic problem - the normal velocity which is related to the normal derivative of pressure. Conversely, the primary variable for the acoustic problem - the pressure, defines the flux for the elasticity problem. This “cross-coupling” is very essential in proving the well-posedness of the problem, and stability of Galerkin approximations.

On top of the interface conditions there are the usual boundary conditions for acoustics,

- prescribed pressure on Γ_{Da},
$$p = p_D$$
- prescribed normal velocity on Γ_{Na},
$$v_n = v_0$$
- an impedance condition with an impedance constant $d > 0$ on Γ_{Ca},
$$v_n = dp + v_0$$

and for the elasticity,

- prescribed displacements on Γ_{De},
$$u_i = u_{i,D}$$
- prescribed tractions on Γ_{Ne},
$$t_i := \sigma_{ij} n_j = g_i$$
- prescribed impedance on Γ_{Ce},
$$t_i + i\omega\beta_{ij} u_j = g_i$$

The derivation of the variational formulation starts with the weak form of the continuity equation for acoustics,

$$\int_{\Omega_a} \left(\frac{i\omega}{c^2} pq - \rho_f \boldsymbol{v} \boldsymbol{\nabla} q \right) \, d\boldsymbol{x} + \rho_f \int_{\partial\Omega_a} v_n q \, dS = 0, \quad \forall q \tag{8}$$

and the weak form of the conservation of momentum for elasticity,

$$\int_{\Omega_e} \left(\sigma_{ij} v_{i,j} - \rho_s \omega^2 u_i v_i \right) \, d\boldsymbol{x} - \int_{\partial\Omega_e} \sigma_{ij} n_j v_i \, dS = \int_{\Omega_e} f_i v_i \, d\boldsymbol{x}, \quad \forall v_i \tag{9}$$

with ρ_s and f_i denoting the density of solid and body forces, respectively. Boundary $\partial\Omega_a$ of the acoustic subdomain is now split into the interface Γ_N and parts $\Gamma_{Da}, \Gamma_{Na}, \Gamma_{Ca}$. For the interface Γ_I, the first interface condition is utilized to replace the flux term $\rho_f v_n$ with $i\omega\rho_f u_n$. The derivation proceed in the standard way with the acoustic boundary conditions, to obtain the variational statement,

$$\begin{cases} p = p_D \text{ on } \Gamma_{Da} \\ \displaystyle\int_{\Omega_a} \left(\frac{i\omega}{c^2} pq + \frac{1}{i\omega} \boldsymbol{\nabla} p \boldsymbol{\nabla} q \right) \, d\boldsymbol{x} + \\ \int_{\Gamma_{Ca}} \rho_f d \, pq \, dS + \\ \int_{\Gamma_I} i\omega\rho_f u_n \, q \, dS = \\ \int_{\Gamma_{Na} \cup \Gamma_{Ca}} \rho_f v_0 q \, dS, \\ \qquad \forall q \, : q = 0 \text{ on } \Gamma_{Da} \end{cases}$$

Similarly, boundary $\partial\Omega_e$ of the elastic subdomain is split into the interface Γ_N and parts $\Gamma_{De}, \Gamma_{Ne}, \Gamma_{Ce}$. For the interface Γ_I, the second interface condition is utilized to replace the flux term $\sigma_{ij} n_j$ with $-pn_i$. The boundary conditions are used to obtain the variational statement,

$$\begin{cases} \boldsymbol{u} = \boldsymbol{u}_D \text{ on } \Gamma_{De} \\ \displaystyle\int_{\Omega_e} \left(E_{ijkl} u_{k,l} v_{i,j} - \rho_s \omega^2 u_i v_i \right) \, d\boldsymbol{x} + \\ i\omega \int_{\Gamma_{Ce}} \beta_{ij} u_j v_i \, dS + \\ \int_{\Gamma_I} p v_n \, dS = \int_{\Omega_e} f_i v_i \, d\boldsymbol{x} + \\ \int_{\Gamma_{Ne} \cup \Gamma_{Ce}} g_i v_i \, dS, \\ \qquad \forall \boldsymbol{v} \, : \boldsymbol{v} = \boldsymbol{0} \text{ on } \Gamma_{De} \end{cases}$$

The final variational formulation for the coupled problem in the form is obtained by multiplying the variational statement for acoustics by factor $i\omega$.

$$\begin{cases} \boldsymbol{u} \in \tilde{\boldsymbol{u}}_D + \boldsymbol{V}, \; p \in \tilde{p}_D + V, \\ b_{ee}(\boldsymbol{u}, \boldsymbol{v}) + b_{ae}(p, \boldsymbol{v}) = l_e(\boldsymbol{v}), \qquad \forall \boldsymbol{v} \in \boldsymbol{V} \\ b_{ea}(\boldsymbol{u}, q) + b_{aa}(p, q) = l_a(q), \qquad \forall q \in V \end{cases} \tag{10}$$

where:

- the bilinear and linear forms are given by the formulas:
$$\begin{aligned} b_{ee}(\boldsymbol{u}, \boldsymbol{v}) &= \int_{\Omega_e} \left(E_{ijkl} u_{k,l} v_{i,j} - \rho_s \omega^2 u_i v_i \right) \, d\boldsymbol{x} + \\ &\quad i\omega \int_{\Gamma_{Ce}} \beta_{ij} u_j v_i \, dS \\ b_{ae}(p, \boldsymbol{v}) &= \int_{\Gamma_I} p v_n \, dS \\ b_{ea}(\boldsymbol{u}, q) &= -\omega^2 \rho_f \int_{\Gamma_I} u_n q \, dS \\ b_{aa}(p, q) &= \int_{\Omega_a} \left(\boldsymbol{\nabla} p \boldsymbol{\nabla} q - k^2 pq \right) \, d\boldsymbol{x} + \\ &\quad i\omega \int_{\Gamma_{Ca}} \rho_f d \, pq \, dS \\ l_e(\boldsymbol{v}) &= \int_{\Omega_e} f_i v_i \, d\boldsymbol{x} + \\ &\quad \int_{\Gamma_{Ne} \cup \Gamma_{Ce}} g_i v_i \, dS \\ l_a(q) &= i\omega\rho_f \int_{\Gamma_{Na} \cup \Gamma_{Ca}} v_0 q \, dS \, , \end{aligned} \tag{11}$$
- $\tilde{\boldsymbol{u}}_D \in \boldsymbol{H}^1(\Omega_e) := (H^1(\Omega_e))^3$ is a finite energy lift of displacements $\boldsymbol{u}_D$ prescribed on Γ_{De}, $\tilde{p_D} \in H^1(\Omega_a)$ is a finite enery lift of pressure p_D prescribed on Γ_{Da},
- $\boldsymbol{V}$ and V are the spaces of the test functions,
$$\begin{aligned} \boldsymbol{V} &= \{ \boldsymbol{v} \in \boldsymbol{H}^1(\Omega_e) \, : \, \boldsymbol{v} = \boldsymbol{0} \text{ on } \Gamma_{De} \} \\ V &= \{ q \in H^1(\Omega_a) \, : \, q = 0 \text{ on } \Gamma_{Da} \} \end{aligned} \tag{12}$$
- $k = \omega/c$ is the acoustic wave number.

Coupled problem 10 is symmetric if and only if diagonal forms b_{ee} and b_{aa} are symmetric and,

$$b_{ae}(p, \boldsymbol{u}) = b_{ea}(\boldsymbol{u}, p) \, .$$

Thus, in order to enable the symmetry of the formulation[2], it is necessarz to rescale problem by, for instance, dividing the second equation by factor $-\omega^2\rho_f$.

III. The Head Problem

In this section the details of the head problem are introduced. The problem falls into the category of general coupled elasticity/acoustics problems discussed in Section II with a few modifications. The domain Ω in which the problem is defined is the interior of a ball including a model of the human head, and it is split again into an acoustic part Ω_a, and an elastic part Ω_e. Depending upon a particular example, the acoustic part Ω_a includes:

- air surrounding the human head, bounded by the head surface and a truncating sphere; this part of the domain may include portions of air ducts leading to the middle ear through mouth and nose openings;
- cochlea,
- an additional layer of air bounded by the truncating sphere and the outer sphere terminating the computational domain, where the equations of acoustics are replaced with the corresponding *Perfectly Matched Layer* (PML) modification.

The elastic part of the domain includes:

- skull,
- tissue.

The term *tissue* is understood here as all parts of the head that are not occupied by the skull (bone) and the cochlea. This includes the thin layer of the skin and the entire interior of the head with the brain. In the current stage of the project it is assumed that the elastic constants for the whole tissue domain are the same.

The acoustic wave is represented as the sum of an incident wave p^{inc} and a scattered wave p. Only the scattered wave is assumed to satisfy the radiation (Sommerfeld) condition,

$$\frac{\partial p}{\partial r} + ikp \in L^2(\mathbb{R}^3) \tag{13}$$

The different types of boundaries discussed in the previous section reduce only to the interface between the elastic and acoustic subdomains and the outer, Dirichlet boundary for the acoustic domain. Material interfaces between the skull and tissue, as well between the air and the PML air do not require any special treatment.

[2]This is essential, among other reasons, from the point of view of using a direct solver.

The final formulation of the problem has the form 10, with the bilinear and linear forms defined as follows.

$$\begin{aligned}
b_{ee}(\boldsymbol{u},\boldsymbol{v}) &= \int_{\Omega_e} \left(E_{ijkl}u_{k,l}v_{i,j} - \rho_s\omega^2 u_i v_i\right)\, d\boldsymbol{x} \\
b_{ae}(p,\boldsymbol{v}) &= \int_{\Gamma_I} p v_n\, dS \\
b_{ea}(\boldsymbol{u},q) &= -\omega^2\rho_f \int_{\Gamma_I} u_n q\, dS \\
b_{aa}(p,q) &= \int_{\Omega_a} \left(\boldsymbol{\nabla} p \boldsymbol{\nabla} q - k^2 pq\right)\, d\boldsymbol{x} \\
l_e(\boldsymbol{v}) &= -\int_{\Gamma_I} p^{inc} v_n\, dS \\
l_a(q) &= 0
\end{aligned} \tag{14}$$

A symmetric formulation is enabled by dividing the equations of acoustics with factor $\rho_f\omega^2$,

$$\begin{aligned}
b_{ee}(\boldsymbol{u},\boldsymbol{v}) &= \int_{\Omega_e} \left(E_{ijkl}u_{k,l}v_{i,j} - \rho_s\omega^2 u_i v_i\right)\, d\boldsymbol{x} \\
b_{ae}(p,\boldsymbol{v}) &= \int_{\Gamma_I} p v_n\, dS \\
b_{ea}(\boldsymbol{u},q) &= -\int_{\Gamma_I} u_n q\, dS \\
b_{aa}(p,q) &= \tfrac{1}{\omega^2\rho_f} \int_{\Omega_a} \left(\boldsymbol{\nabla} p \boldsymbol{\nabla} q - k^2 pq\right)\, d\boldsymbol{x} \\
l_e(\boldsymbol{v}) &= -\int_{\Gamma_I} p^{inc} v_n\, dS \\
l_a(q) &= 0
\end{aligned} \tag{15}$$

Notice that the outer normal unit vector $\boldsymbol{n}$ is refered always *locally*, i.e. in the formula for the coupling bilinear form b_{ae} involving elasticity test functions $\boldsymbol{v}$, versor $\boldsymbol{n}$ points outside of the elastic domain, whereas in the formula for the coupling bilinear form b_{ea} involving acoustic test functions q, versor $\boldsymbol{n}$ points outside of the acoustic domain. The normal components v_n and u_n present in the coupling terms are thus opposite to each other, and the formulation is indeed symmetric.

a) PML modification: In the PML part of the acoustical domain, the bilinear form b_{aa} is modified as follows:

$$b_{aa}(p,q) = \int_{\Omega_{a,PML}} \left(\frac{z^2}{z'r^2}\frac{\partial p}{\partial r}\frac{\partial q}{\partial r} + \frac{z'}{r^2}\frac{\partial p}{\partial \psi}\frac{\partial q}{\partial \psi} + \frac{z'}{r^2\sin^2\psi}\frac{\partial p}{\partial \theta}\frac{\partial q}{\partial \theta}\right) r^2 \sin\psi\, dr\, d\psi\, d\theta \tag{16}$$

Here r, ψ, θ denote the standard spherical coordinates and $z = z(r)$ is the PML stretching factor defined as follows,

$$z(r) = (1 - \frac{i}{k}\left[\frac{r-a}{b-a}\right]^{\alpha})r \tag{17}$$

Here a is the radius of the truncating sphere, b is the external radius of the computational domain ($b-a$ is thus the thickness of the PML layer), i denotes the imaginary unit, k is the acoustical wave number, and r is the radial coordinate. In computations, all derivatives with respect to spherical coordinates are expressed in terms of the standard derivatives with respect to Cartesian coordinates. In all reported computations, parameter $\alpha = 5$. For a detailed discussion on derivation of PML modifications and effects of higher order discretizations see [7].

IV. Finite Element Discretization and Implementation Details

Except for the PML domain, both acoustic and elastic domains are discretized with the simplest linear tetrahedra, i.e. pressure p and elastic displacement components u_i are linear within each element. This implies that all interfaces including the truncating sphere are approximated with plane triangular panels. The triangular mesh on the (approximate) truncating sphere is extended in the radial direction to form two layers of prismatic elements. In order to approximate well the PML induced layer, higher order polynomials in the radial direction are used, $p = 4$ in the first layer, and $p = 2$ in the second layer. This is in accordance with our experience of resolving PML induced boundary layers with hp-adaptive elements, see [7] for examples.

A. Generation of tetrahedral meshes

The numerical examples presented in this paper utilize computational meshes obtained from MATLAB based mesh generator [8], modified to fit into our problem.

The mesh is described in the following files:

- *sphere_file* - contains a list of vertices and triangles on the truncating sphere,
- *tissue_skull_file* - contains a list of vertices and triangles on the tissue/skull interface,
- *air_skull_file* - contains a list of vertices and triangles on the air/skull interface,
- *cochlea_air_file* - contains a list of vertices and triangles on the cochlea/air interface,
- *cochlea_file* - contains a list of vertices and tetrahedra within the cochlea,
- *air_file* - contains a list of vertices and tetrahedra within air,
- *skull_file* - contains a list of vertices and tetrahedra within skull,
- *tissue_file* - contains a list of vertices and tetrahedra within tissue

The meshes are fully compatible, i.e. for instance all vertices for the skull tetrahedra, that are located on the skull/air interface, coincide with vertices listed in *air_skull_file*.

B. Data structure and element computations

An existing data structure for higher order hexahedral elements, see [3], [4], has been extended to the case of tetrahedral and prismatic elements. The data structure arrays are initiated with a relevant information on nodal connectivities, and element neighbors necessary for element computations.

Element matrices corresponding to bilinear forms are integrated using standard Gaussian quadrature for tetrahedra (volume integrals) and triangles (interface terms).

C. Solvers

Two linear solvers are used in this project. The first one is a serial frontal solver developed at ICES[3] [5], [13], the second one is the European MUMPS, see [8]. The third parallel direct solver is developed, dedicated for hp finite elements. The solver is currently working with two dimensional rectangular elements [10], and three dimensional hexahedral elements [9]. The solver will be extended for three dimensional tetrahedral elements, utilized in this project.

D. Graphics

To visualize the models, meshes and solutions, a simple interface to the Visualization Toolkit (VTK) [12] has been implemented. The VTK is a collection of C++ classes that implement a wide range of visualization algorithms. The central data structure for this project is the `vtkUnstructuredGrid`, which represents volumetric data as a collection of points with corresponding scalar values (in this case, the real and imaginary part of the pressure), connected by cells of arbitrary type and dimension (i.e. lines, triangles, quads, tetrahedra, prisms, etc.). This data is then plugged into a variety of filters that allow us to, for example, "slice" through the dataset with a plane to see the pressure in the interior, extract colored isocontours or isosurfaces of the pressure, or generate an animation of the time-dependent pressure $P(x,t) = \Re(e^{i\omega t} p(x))$.

V. Verification

The code has been verified by implementing so-called manufactured solutions. This is a standard technique in finite elements. It is done by assuming an analytical solution of any form (the manufactured solution), and using the differential equations for both acoustics and elasticity parts, boundary and interface conditions, to compute the corresponding volume forces and boundary fluxes. The verification is invaluable. If a solution that can be reproduced exactly with the FE shape functions is assumed, the corresponding error must be equal to machine zero, in our case values around 10^{-14}. Any values bigger than these, indicate a bug in the code. Values around 10^{-7} indicate a loss of double precision. In our case, due to the use of linear elements in the acoustic domain and linear or quadratic elements in the elastic part, any linear variation for pressure, and any linear(quadratic) variation for displacement vector can be assumed. To verify the code, a simple example of domain consisting of a unit sphere, surrounded with a unit layer of air, and a PML layer of thickness equal to two units is assumed. The sphere was meshed with just eight octant tetrahedra, and the air layer with 8×3 tetrahedra obtained by splitting eight prisms, each into three tetrahedra. The PML layer was modeled with two layers of prismatic elements with arbitrary order $p = 4$ in the radial direction. All material data were set to O(1) values. A typical result of the verification for a mesh with quadratic elements in the elastic domain, is shown in Fig. 2. The same verification technique was then use to verify each data set and/or the three different solvers

[3]The solver was developed by Dr. Eric Becker, a professor in the ASE/EM Dept. and a long time member of TICOM, next TICAM and now ICES

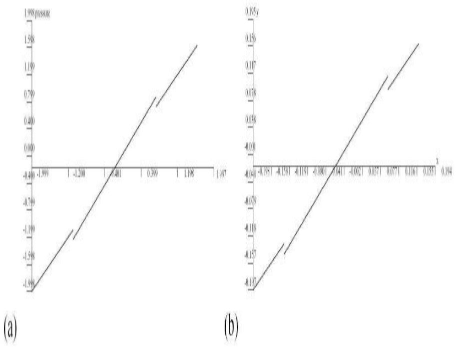

Fig. 2. Verification of the code using a manufactured solution. Pressure distribution along a section passing through the origin and parallel to the x-axis for (a) unit sphere test, and (b) Example 1 with unit material data. Numerical and exact(manufactured) solutions are indistinguishable.

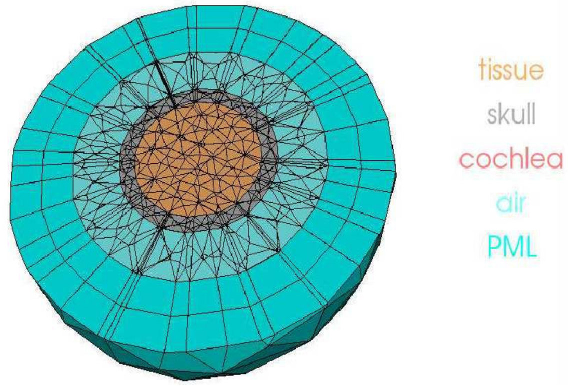

Fig. 3. The ”small” mesh used to solve the multilayer sphere problem.

used for the project: frontal solver, MUMPS, and the parallel nested dissections multifrontal solver. For small data sets, an additional verification is done by comparing results obtained with the different solvers.

VI. Examples

For the further verificiation of the model, the problem of scattering of a plane wave on an elastic, multilayer sphere has been solved. The spherical computational grids have been generated by using the MATLAB mesh generator [11].

In this model, the domain consists of four concentric spheres. The most inner sphere is filled with an elastic material with data corresponding to human brain. The first layer is also elastic with constants corresponding to human skull. The second layer corresponds to air, and the last one to the PML air. The incident wave is assumed in the form of a plane wave impinging from the top,

$p^{inc} = p_0 e^{ikex}$, $e = (0, 0, -1)$, $p_0 = 1[Pa]$ (3.8)

The test problem is being solved with frequency f = 200 Hz. The precise geometry data are as follows:

brain $r < 0.1m$
skull $0.1m < r < 0.125m$
air $0.125m < r < 0.2m$
PML air $0.2m < r < 0.3m$

Three tetrahedral meshes for the interior tissue ball, of radius 10cm ,were generated using the simple MATLAB code distmesh, described in [7]. The surface of this mesh was then manually extended to generate a skull annulus of thickness 2.5cm, surrounding air of thickness 7.5cm, and a PML of thickness 10cm. The problem was solved on three meshes shown in Figures 3, 4, and 5. The meshes will be called ”small”, ”big”, and ”huge”. For all runs discussed for this example, the MUMPS solver has been used. Fig. 6 displays the distribution of the real part of the pressure over plane y = 0 passing through the origin. It looks ”good”. Unfortunately, a similar picture for the imaginary part reveals a severe instability in the ”tissue” region. To double check the VTK graphics, the results have been displayed across a vertical section passing through the origin. The results are shown in Fig. 7. In order to access the problem, the same example has

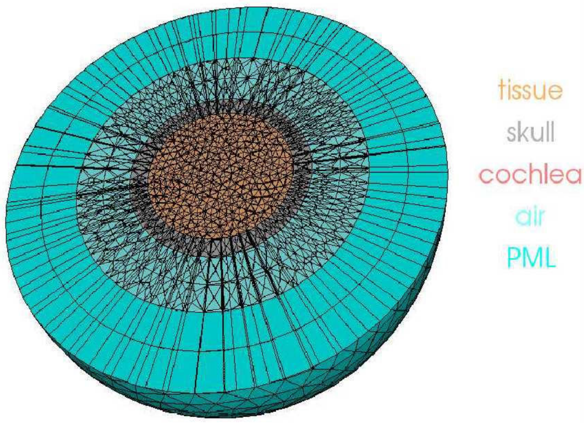

Fig. 4. The ”big” mesh used to solve the multilayer sphere problem.

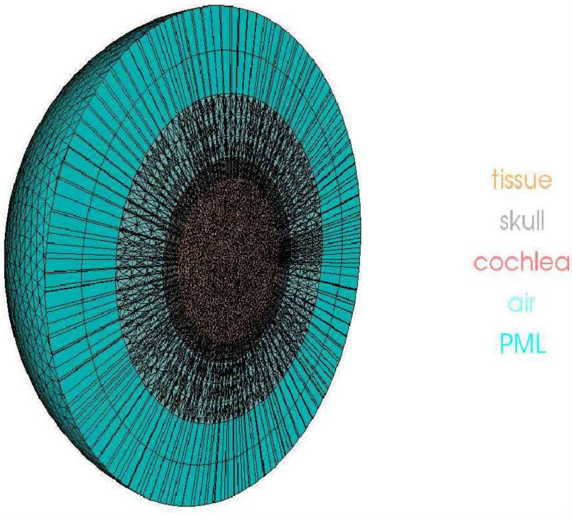

Fig. 5. The ”huge” mesh used to solve the multilayer sphere problem.

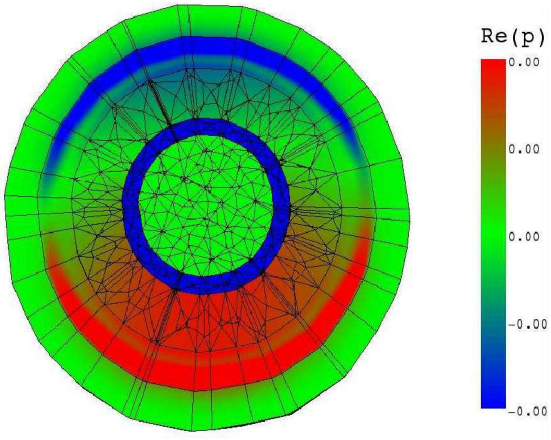

Fig. 6. The concentric spheres problem. Small mesh. Plot of real part of pressure on plane y = 0 passing through origin.

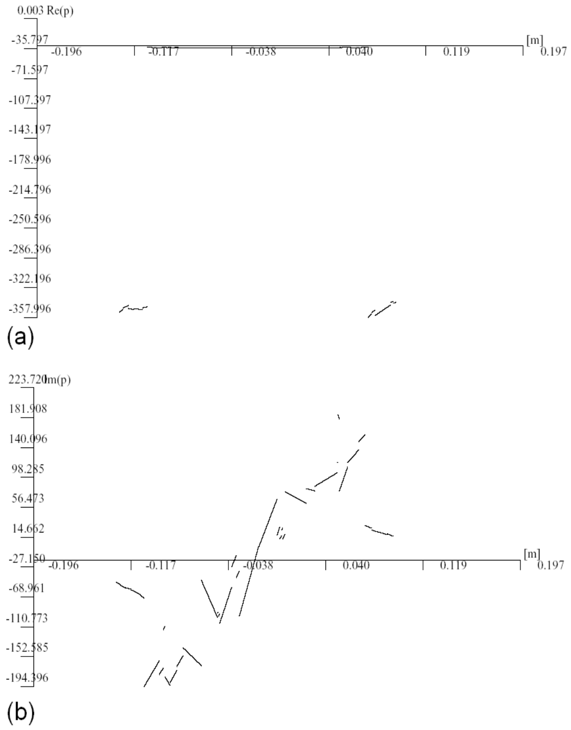

Fig. 7. The concentric spheres problem. Small mesh. Plots of real and imaginary part of pressure along the vertical section.

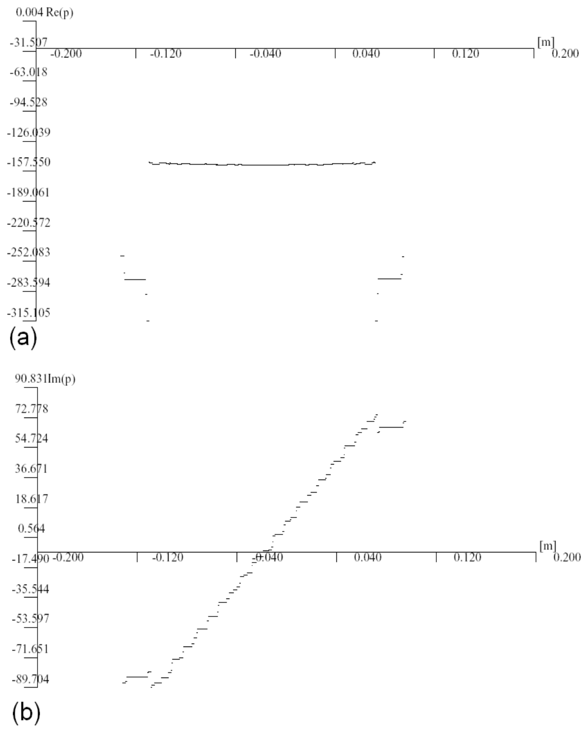

Fig. 8. The concentric spheres problem. Small mesh. Plots of real and imaginary part of pressure along the vertical section for the case of a "stiffer" tissue.

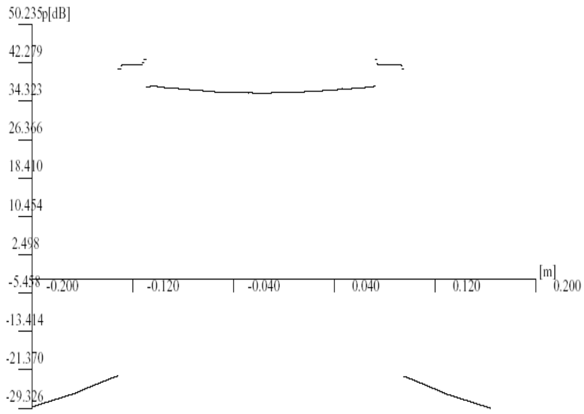

Fig. 9. The concentric spheres problem. Small mesh. Plot of pressure along the vertical section in dB for the case of a "stiff" tissue.

been executed, but with the Young modulus for the tissue domain increased by two orders of magnitude, i.e. E = 67 [MPa]. The corresponding results are shown in Fig. 8. Figure 9 displays the same pressure in dB. Figures 10 and 11 display the same pressure but this time obtained on the big and huge meshes. The values are at the same level which indicates a converged solution. Finally, Figures 12 and 13 display the distribution of real and imaginary parts of the pressure over the y = 0 section obtained on the big mesh. Figures 14 and 15 display the distribution of real and imaginary parts of the pressure over the $y = 0$ section obtained on the big mesh rescaled to values from $-.00001$ to $.00001$ for the real part, and from $-.0001$ to $.0001$ for the imaginary part.

The statistics for the largest mesh on which the code has been we succesfully run is as follows.

number of tets = 890144
number of tissue tets = 183872
number of skull tets = 353136
number of cochlea tets = 0
number of air tets = 353136
number of PML prisms = 16816
total number of d.o.f. = 430566

World Academy of Science, Engineering and Technology
International Journal of Physical and Mathematical Sciences
Vol:2, No:12, 2008

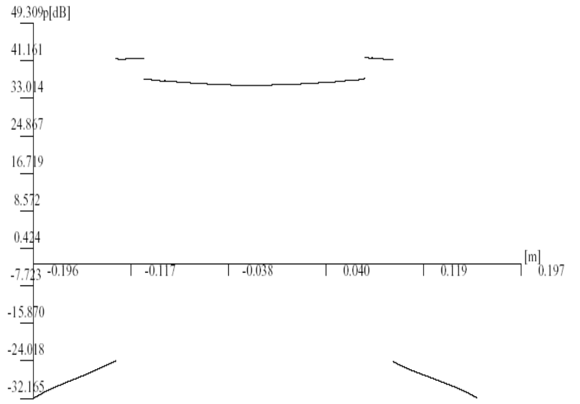

Fig. 10. The concentric spheres problem. Big mesh. Plot of pressure along the vertical section in dB for the case of a "stiff" tissue.

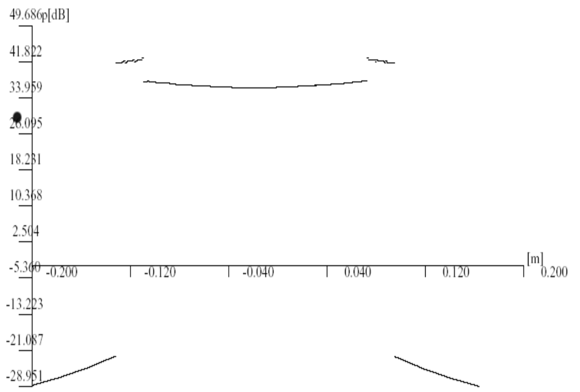

Fig. 11. The concentric spheres problem. Huge mesh. Plot of pressure along the vertical section in dB for the case of a "stiff" tissue.

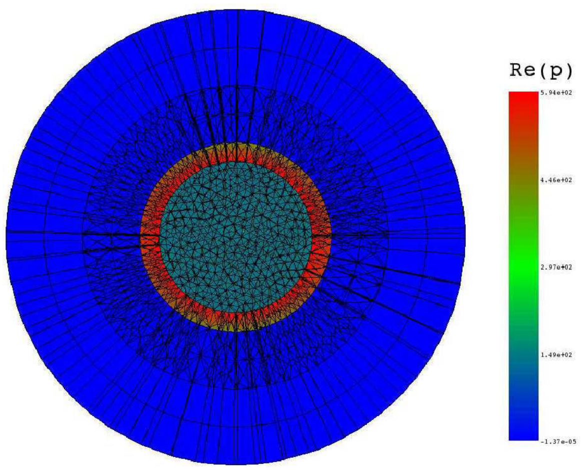

Fig. 12. The concentric spheres problem. Big mesh. Plot of real part of pressure on plane $y = 0$ passing through origin.

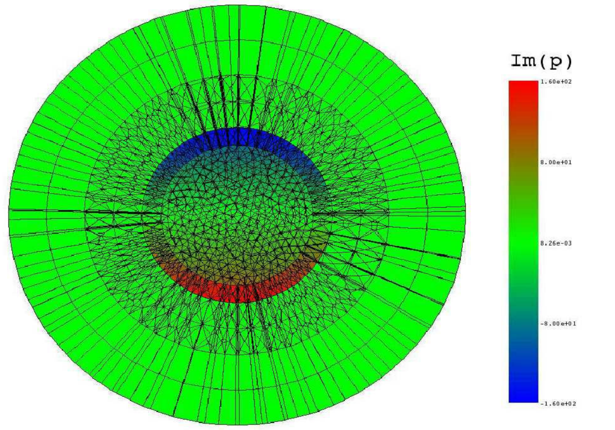

Fig. 13. The concentric spheres problem. Big mesh. Plot of imaginary part of pressure on plane $y = 0$ passing through origin.

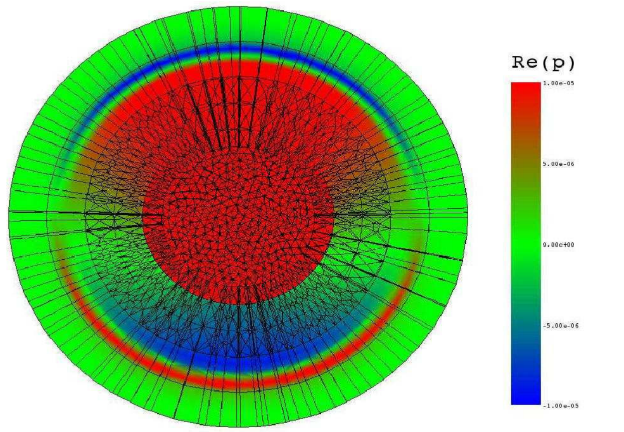

Fig. 14. The concentric spheres problem. Big mesh. Plot of real part of pressure on plane $y = 0$ passing through origin, in the range -0.00001 to 0.00001.

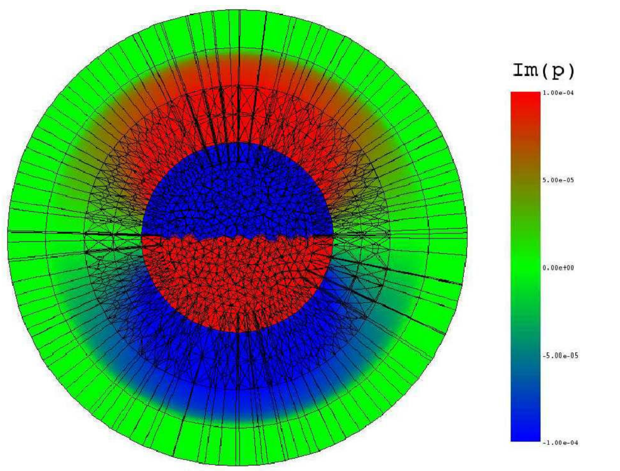

Fig. 15. The concentric spheres problem. Big mesh. Plot of imaginary part of pressure on plane $y = 0$ passing through origin, in the range -0.0001 to 0.0001.

VII. Conclusion

This paper presented a new veriational formulation for coupled elasticity/acoustics problems is presented. The formulation was implemented within the finite element method code with linear and second order three dimensional tetrahedral elements. The code was verified with the manufactured solution technique. A sequence of computational problems with concentric multi-layer spheres representing the tissue, skull and the air, was solved. The computational meshes were generated by MATLAB based mesh generator.

The first direction of the future work will include developing more sophisticated mesh generator, based on MRI scan data. The octree-based isocontouring method [15] to extract interior and exterior tetrahedral meshes for the acoustic and elastic domains will be utilized. Compared to other tetrahedral extraction methods from imaging data, this method generates adaptive and quality 3D meshes without introducing any hanging nodes. The second direction of the future research will be the incorporation of the code with the parallel solver [10], [9]. The third direction will be enhancing the code with mesh refinements technique, based on our experience with hexahedral grids [4].

Acknowledgment

The work of the first authour has been partially supported by the Foundation for Polish Science under Homing programme, and by the Polish Ministry of Scientific Research and Information Technology grant no. NN519 318635.

References

[1] H. Kopka and P. W. Daly, *A Guide to LaTeX*, 3rd ed. Harlow, England: Addison-Wesley, 1999.
[2] Y.C. Chang and L. Demkowicz, Scattering on a spherical shell problem. Comparison of 3D elasticity and Kirchhoff shell theory results. *Computer Assisted Mechanics and Engineering Science*, 2:207229, 1995.
[3] L. Demkowicz. *Computing with hp Finite Elements. I.One- and Two-Dimensional Elliptic and Maxwell Problems*. Chapman & Hall/CRC Press, Taylor and Francis, 2006.
[4] L. Demkowicz, J. Kurtz, D. Pardo, M. Paszyński, W. Rachowicz, and A. Zdunek, *Computing with hp Finite Elements. II Frontiers: Three-Dimensional Elliptic and Maxwell Problems with Applications*. Chapman & Hall/CRC Press, Taylor and Francis, 2007.
[5] P. Geng, J.T. Oden, and R.A. van de Geijn. A parallel multifrontal algorithm and its implementation. *Computer Methods in Applied Mechanics and Engineering*, 149:289301, 1997.
[6] A. Majda. Compressible Fluid Flow and Systems of Conservation Laws in Several Space Variables, *volume 53 of Applied Mathematical Sciences*, Springer-Verlag, New York, 1984.
[7] Ch. Michler, L. Demkowicz, J. Kurtz, and D. Pardo. Improving the performance of perfectly matched layers ny means of hp-adaptivity. *ICES-Report*, 06-17, The University of Texas at Austin, 2006.
[8] *MUMPS: a multifrontal massively parallel sparse direct solver*, http://www.enseeiht.fr/lima/apo/MUMPS/.
[9] M. Paszyński, Performance of Multi Level Parallel Direct Solver for hp Finite Element Method, *Lecture Notes in Computer Science*, 4967:1303-1312, 2007.
[10] M. Paszyński, D. Pardo, C. Torres-Verdin, L. Demkowicz, and V. Calo, A Multi-Level Direct Substructuring Multi-Frontal Parallel Direct Solver for hp-Finite Element Method, *ICES-Report*, 07-33, The University of Texas at Austin, 2007
[11] P.-O. Persson and G. Strang. A simple mesh generator in matlab. *SIAM Review*, 46(2):329 345, 2004.
[12] W. Schroeder, K. Martin and B. Lorensen. The Visualization Toolkit An Object-Oriented Approach To 3D Graphics, 3rd Edition. *Kitware, Inc.*, (http://www.kitware.com).
[13] T. Walsh and L. Demkowicz. A parallel multifrontal solver for hp-adaptive finite elements. *Technical Report 1, TICAM*, The University of Texas at Austin, 1999.
[14] T. Walsh, L. Demkowicz and R. Charles. Boundary element modeling of the external human auditory system. *J. Acoust. Soc. Am.*, 115(3), 2004.
[15] Y. Zhang, C. Bajaj, and B-S Sohn. 3D finite element meshing from imaging data. *The special issue of Computer Methods in Applied Mechanics and Engineering (CMAME) on Unstructured Mesh Generation*, 194(48-49):50835106, 2005.

Maciej Paszyński received his Ph.D. (2003) in Mathematics with applications to Computer Science from the Jagiellonian University, Cracow, Poland. In 2003-2005, he worked as a Postdoctoral Fellow at the Institute for Computational Engineering and Sciences (ICES) at The University of Texas at Austin. In 2005-2006, he worked at the Department of Modeling and Information Technology at AGH University of Science and Technology of Cracow. In Summer 2006, he worked as a Postdoctoral Fellow at the Department of Petroleum and Geosystems Engineering at The University of Texas at Austin. Since 2006, he holds a position as an Assistant Professor in the Department of Computer Science at AGH University of Science and Technology of Cracow. His research interests include parallel self-adaptive two and three dimensional hp finite element method, parallel direct solvers, computational electromagnetics and material science.

Leszek Demkowicz is a Professor in the Department of Aerospace Engineering and Engineering Mechanics at The University of Texas at Austin. Since 1993, he has served as an Assistant Director of the Institute for Computational Engineering and Sciences (ICES) at The University of Texas at Austin. He graduated cum laudae from Cracow University of Technology in 1976 with M.S. in Engineering Mechanics and from Jagiellonian University in Cracow in 1978 with M.S. in Theoretical Mathematics. He received a Ph.D.in Engineering in 1982 from The Cracow University of Technology, Poland. Dr. Demkowicz edited two books, has authored and co-authored two books, has published over 100 papers, and over 35 technical reports (unpublished elsewhere). He serves on the editorial board of four international journals. His area of expertise includes Functional Analysis, Numerical Analysis, h, p, and hp Adaptive Finite Element Methods with applications to solid and fluid mechanics, elasticity, acoustics and electromagnetic wave propagation.

Jason Kurtz received his Ph.D.(2007) in Computational and Applied Mathematics from The University of Texas at Austin. He currenty works as a Postdoctoral Fellow at The University of Texas at Austin. His research interests include fully automatic hp adaptivity in three dimensions, direct solvers for h and hp adaptive finite element method, computational electromagnetics.